

Supplement of "A Chemical Ionization Mass Spectrometry Utilizing Ammonium Ions (NH_4^+ CIMS) for Measurements of Organic Compounds in the Atmosphere"

Xu et al.

Correspondence: Lu Xu (lu.xu@noaa.gov) and Carsten Warneke (carsten.warneke@noaa.gov)

1 Mass-Dependent Transmission Efficiency

During transport, ions get lost in the BSQ, in the ion guides, and in the extraction region of the ToF. In this study, the mass-dependent transmission efficiency is defined as the fraction of ions reaching the mass analyzer in the total ions exiting the FIMR. We experimentally quantify the mass-dependent transmission efficiency relative to the reagent ion $\text{NH}_4^+ \cdot \text{H}_2\text{O}$ by introducing a series of compounds spanning a range of molecular weight (32 - 370 m/Q) in a large enough quantity to deplete the fraction of reagent ions by $\sim 20\text{-}30\%$ (Huey et al., 1995; Heinritzi et al., 2016). The ratio of the increase of the product ions to the decrease of the reagent ion indicates the relative transmission efficiency between these two masses. The mass-dependent transmission efficiency is obtained under similar condition as ambient measurements, where $\text{NH}_4^+ \cdot \text{H}_2\text{O}^+$ is the dominant reagent ion with the presence of NH_4^+ . In the following derivation, $[X]$ represents the observed signal of ion X by the mass analyzer and TE represents its transmission efficiency. Hence, $[X]/\text{TE}_X$ represents the X signal in the FIMR. We consider reactions of analyte M with both $\text{NH}_4^+ \cdot \text{H}_2\text{O}$ (Eqn. S1) and NH_4^+ (Eqn. S2). Based on ion balance, the production of product ions equals the loss of reagent ions in the FIMR (Eqn. S3). Because of the bandpass properties of the BSQ, the NH_4^+ signal is not observable. Thus, we assume the ratio of the consumption rate of M with NH_4^+ to that with $\text{NH}_4^+ \cdot \text{H}_2\text{O}$ is α (i.e., Eqn. S4). Further, we assume that all the product ions from the same analyte have the same TE. This assumption is reasonable based on the observations that clustering with NH_4^+ is the dominant product for the analytes selected in this calibration and that other product ions are within the 20 amu of the parent ion. Based on these two assumptions, the Eqn. S3 is simplified to Eqn. S5. For each analyte, its concentration is varied to obtain a range of $\sum \Delta[\text{P}_i]$ and $\Delta[\text{NH}_4^+ \cdot \text{H}_2\text{O}]$, which are linearly fitted. The slope represents the transmission efficiency of the parent ion relative to that of $\text{NH}_4^+ \cdot \text{H}_2\text{O}$. Finally, the relative transmission efficiency is normalized to that of hydroxyacetone. The mass range below 101 amu is fitted with a Hill Equation and the above 101 amu is linearly fitted. The mass-dependent transmission curve is shown in Figure S1.



$$\sum \frac{\Delta[\text{P}_i]}{\text{TE}_{\text{P}_i}} = \frac{\Delta[\text{NH}_4^+ \cdot \text{H}_2\text{O}]}{\text{TE}_{\text{NH}_4^+ \cdot \text{H}_2\text{O}}} + \frac{\Delta[\text{NH}_4^+]}{\text{TE}_{\text{NH}_4^+}} \quad (\text{S3})$$

$$\frac{\Delta[\text{NH}_4^+]}{\text{TE}_{\text{NH}_4^+}} = \alpha \frac{\Delta[\text{NH}_4^+ \cdot \text{H}_2\text{O}]}{\text{TE}_{\text{NH}_4^+ \cdot \text{H}_2\text{O}}} \quad (\text{S4})$$

$$25 \quad \sum \Delta[\text{P}_i] = (1 + \alpha) \frac{\text{TE}_{\text{M} \cdot \text{NH}_4^+}}{\text{TE}_{\text{NH}_4^+ \cdot \text{H}_2\text{O}}} \Delta[\text{NH}_4^+ \cdot \text{H}_2\text{O}] \quad (\text{S5})$$

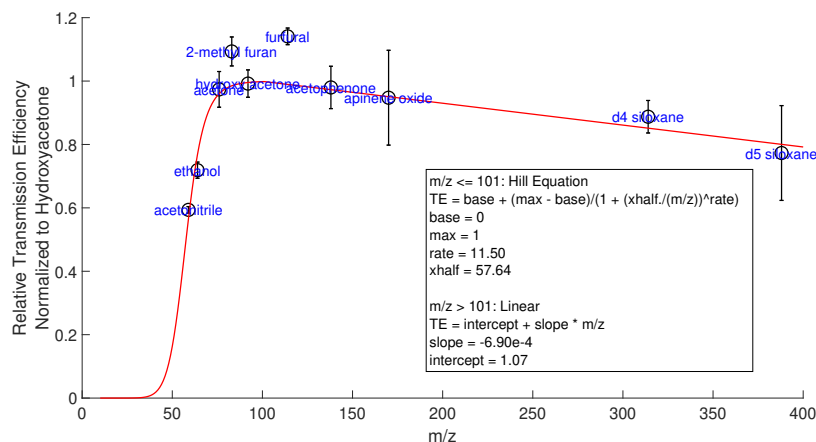


Figure S1. Mass-dependent transmission efficiency. The m/z includes the NH_4^+ reagent ion. Note that the transmission efficiency for ions smaller than m/z 59 is not constrained.

2 Vocus Inlet Design

When sampling gas phase in the field deployment, ambient air is drawn at 3 standard liter per minute (slpm) through a 10 m long PFA tubing (OD 1/4 inch and ID 3/16 inch), from which the Vocus sub-sampled with a flow rate of 0.1 slpm. The residence time in the main tubing is 6 s. This residence time is not optimal and could potentially cause sampling losses of low volatility species. Higher flow rate causes challenge in maintaining the FIMR pressure at the targeted value (3 mbar), because of the Vocus inlet design. There are two options to sub-sample from the main flow, using the 1/4 inch stainless steel fitting on the center of Vocus or using the 1/16 inch side port on the high-pressure side of the Vocus inlet. Because the center port is reserved and later used for particle measurement in the campaign, the 1/16 inch side port is used for gas sampling. As a result, this 1/16 inch port and the associated 1/16 inch tubing restrict the flow and cause a large pressure drop from the main sample flow to the instrument. Larger main flow rate decreases the pressure in the sampling line and causes that the FIMR pressure can not reach the targeted value under current design of the vacuum system. Further improvements of the Vocus inlet and the vacuum system are required in order to sample both gas and particles with larger main flow rate.

3 Voltage Scan Procedure to Probe the Stability of Product Ions

To probe the stability of product ions, we performed voltage scanning test following the procedure outlined in Lopez-Hilfiker et al. (2016) and Zaytsev et al. (2019). In brief, we vary the voltage gradient between FIMR back and skimmer (ΔV ranges from 5 to 80 V) while keeping the voltage gradient upstream of the FIMR back constant. Larger ΔV increases the collisional energy and causes stronger collision-induced dissociation of product ions. As a result, the signal of product ions decreases with increasing ΔV . We define ΔV_{50} as the voltage gradient at which the parent ion signal drops to half of the maximum signal. The ΔV_{50} is converted to the kinetic energy of product ions in the center of mass ($KE_{cm,50}$), which is a measure of their stability, following the calculation below. The electric field strength (E) between the FIMR back and skimmer is calculated using Eqn. S6, where d is the distance between the FIMR back and skimmer. The accurate value of d is unknown, and it is assumed to be 3 mm in the calculation. This assumption affects the absolute value of $KE_{cm,50}$ of individual analyte, but not the relative difference in $KE_{cm,50}$ between different analytes, because d is the same for all analytes. The drift velocity of ion (v_d) between FIMR back and skimmer is determined by E and the ion mobility. It is calculated using Eqn. 10. The mean kinetic energy of drifting ion (KE_{ion}) is calculated using Eqn. S7, where m_{buffer} and m_{ion} represent the mass of buffer gas and ion. Finally, the kinetic energy of ion in the center of mass ($KE_{cm,50}$) is calculated using Eqn. S8.

Figure S2 shows the dependence of parent ions of nearly 60 analytes on the ΔV . On one hand, increasing the ΔV leads to declustering and lower signal. On the other hand, increasing ΔV affects the ions transmission between FIMR back and skimmer. The observation in Figure S2 is a combination of both effects. This explains why signals of some analytes show an initial increase as ΔV increases.

The signal of d5 siloxane does not drop to half of the maximum signal even at the largest ΔV . This suggests it has a strong binding energy with NH_4^+ . Because of a lack of ΔV_{50} measurement, d5 siloxane is not included in the analyzing relationship between S_{corr} and $KE_{cm,50}$. Further, the dipoment and polarizability of d5 siloxane are also challenging to theoretically calculate.

$$E = \frac{\Delta V_{50}}{d} \quad (S6)$$

$$KE_{ion} = \frac{3}{2} k_B T_{FIMR} + \frac{m_{buffer} v_d^2}{2} + \frac{m_{ion} v_d^2}{2} \quad (S7)$$

$$KE_{cm,50} = \frac{m_{buffer}}{m_{buffer} + m_{ion}} (KE_{ion} - \frac{3}{2} k_B T_{FIMR}) + \frac{3}{2} k_B T_{FIMR} \quad (S8)$$

4 Modeling the Ion Distribution

The reactions between $H_3O^+ \cdot (H_2O)_n$ ($n = 0,1,2$) and NH_3 are treated as irreversible, while all the other reactions in Figure S3 are reversible. This is because the proton affinity of NH_3 (i.e., 853.6 kJ mol⁻¹ from Hunter and Lias (1998)) is larger than that of

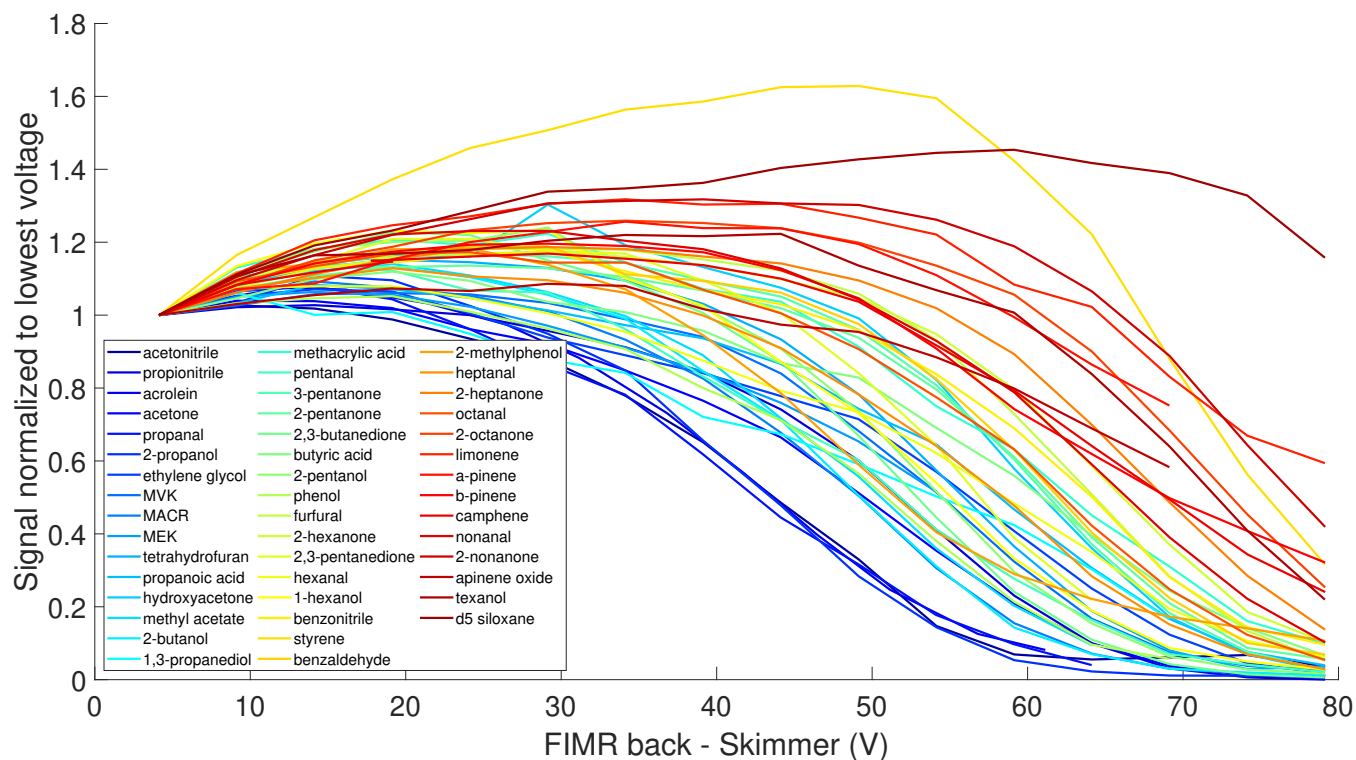


Figure S2. The dependence of analyte signal on the voltage gradient between FIMR back and skimmer. The analyte signal is normalized to that measured at the lowest voltage gradient. Only analytes with sensitivity larger than 50 cps ppbv⁻¹ are shown here.

H₂O (i.e., 691 kJ mol⁻¹ from Hunter and Lias (1998)) and (H₂O)₂ (832.7 kJ mol⁻¹ from Kawai et al. (2003)), so that the reverse reactions are negligible. (H₂O)₃ has larger proton affinity (888.6 kJ mol⁻¹ from theoretical calculation in Kawai et al. (2003)) than NH₃. However, treating the reaction between H₃O⁺ · (H₂O)₂ and NH₃ as reversible leads to significantly lower amounts of NH₄⁺ · H₂O compared to the observations. In contrast, treating this reaction as irreversible (i.e., producing NH₄⁺) leads to more realistic results. This treatment is reasonable given the uncertainties in the calculated proton affinity of (H₂O)₃. Finally, the time-dependent concentrations of all ions in Figure S3 are obtained by solving a set of ordinary differential equations (ODEs). The simulation time, which is the ion-molecule reaction time, is on the order of 100 μs. It is calculated based on the FIMR length (10 cm) and the calculated ion velocity (Eqn. 10) under given a FIMR condition.

The NH₃/H₂O ratio is estimated based on the flow rates and the NH₄OH solution concentration. A gas mixture comprised of 20 sccm H₂O and 1 sccm NH₃ + H₂O is introduced into the ion source. The volume concentration of the ammonium hydroxide water solution is 0.5%. Using Raoult's law and the saturation vapor pressures of NH₃ and H₂O at 30°C (i.e., 1.17 × 10⁴ Pa and 4.25 × 10³ Pa, respectively), the 1 sccm gas mixture contains 74% NH₃ and 26% H₂O. Combined with the 20 sccm H₂O flow, the NH₃/H₂O ratio is estimated to be 1.8%. However, this estimation is likely biased high, because it does not account for NH₃ loss to wall reservoirs. In addition, using this estimated ratio leads to substantially higher fraction of NH₄⁺ · NH₃ in the

80 kinetic model than observation. As shown in Figure S4a, when the $\text{NH}_3/\text{H}_2\text{O}$ ratio is 1.8%, the $\text{NH}_4^+ \cdot \text{NH}_3$ is more abundant than $\text{NH}_4^+ \cdot \text{H}_2\text{O}$ when E/N is below 70 Td in the simulation. This contradicts the observation that $\text{NH}_4^+ \cdot \text{H}_2\text{O}$ is more abundant. In Figure S4b, a lower $\text{NH}_3/\text{H}_2\text{O}$ ratio leads to result consistent with the observation. Therefore, we select 0.18% as the start point in the kinetic simulation.

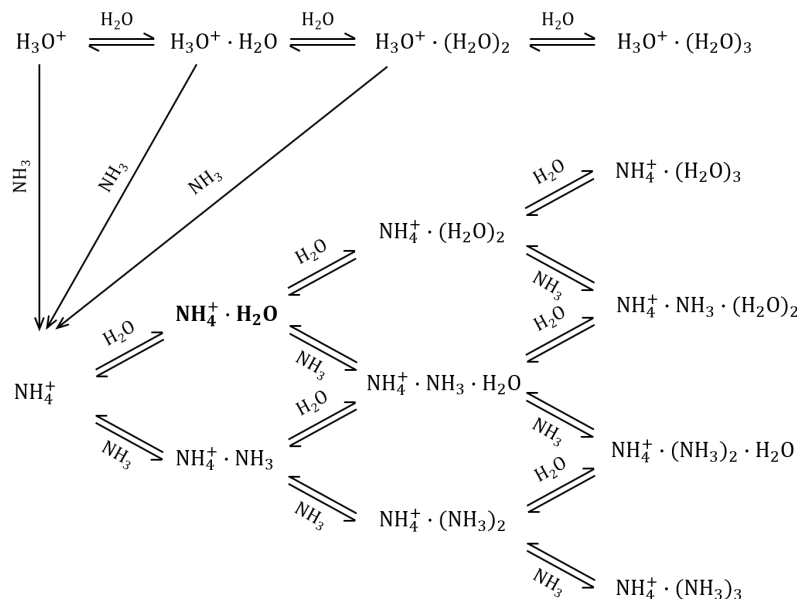


Figure S3. Ion-Molecule reactions in the $\text{H}^+ - \text{NH}_3 - \text{H}_2\text{O}$ system. $\text{NH}_4^+ \cdot \text{H}_2\text{O}$ is the desired reagent ion.

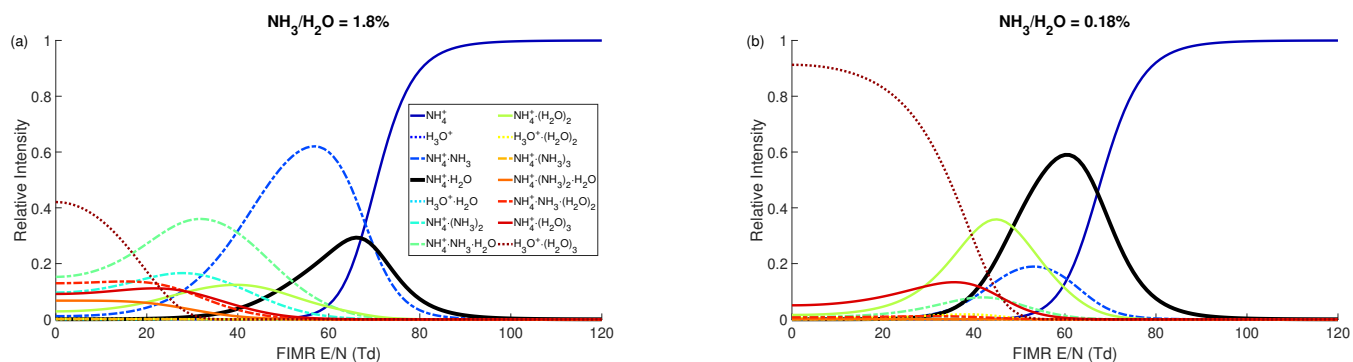


Figure S4. Impacts of $\text{NH}_3/\text{H}_2\text{O}$ ratio on the cluster ion distribution. The simulations are conducted under constant FIMR P (5 mbar), T (330 K), H_2O mixing ratio (0.25%), $\text{NH}_3/\text{H}_2\text{O}$ ratio, but varying E/N . The $\text{NH}_3/\text{H}_2\text{O}$ ratio is 1.8% in panel (a) and 0.18% in panel (b).

To better understand the temperature-dependent sensitivities, we add the reversible reactions of acetone and α -pinene with $\text{NH}_4^+ \cdot \text{H}_2\text{O}$ to the kinetic model and simulate the dependence of their sensitivities on temperature. The NH_4^+ affinities of α -pinene, H_2O , and acetone are 75, 86, and 110 kJ mol^{-1} , respectively. Thus, the reaction enthalpies for acetone + $\text{NH}_4^+ \cdot \text{H}_2\text{O}$

Table S1. Reaction thermochemistry data

	Ion	Neutral	Product	$\Delta_r H^0$ (kJ mol ⁻¹) ¹	$\Delta_r S^0$ (J mol ⁻¹ K) ¹
R1	NH ₄ ⁺	H ₂ O	NH ₄ ⁺ · H ₂ O	-80.6	-94
R2	NH ₄ ⁺	NH ₃	NH ₄ ⁺ · NH ₃	-107	-111
R3	NH ₄ ⁺ · H ₂ O	H ₂ O	NH ₄ ⁺ · (H ₂ O) ₂	-63.9	-101.2
R4	NH ₄ ⁺ · H ₂ O	NH ₃	NH ₄ ⁺ · NH ₃ · H ₂ O	-77	-96.2
R5	NH ₄ ⁺ · NH ₃	H ₂ O	NH ₄ ⁺ · NH ₃ · H ₂ O	-54	-84.9
R6	NH ₄ ⁺ · NH ₃	NH ₃	NH ₄ ⁺ · (NH ₃) ₂	-70.5	-102.2
R7	NH ₄ ⁺ · (H ₂ O) ₂	H ₂ O	NH ₄ ⁺ · (H ₂ O) ₃	-54.8	-99.2
R8	NH ₄ ⁺ · (H ₂ O) ₂	NH ₃	NH ₄ ⁺ · NH ₃ · (H ₂ O) ₂	-76.1	-127
R9	NH ₄ ⁺ · NH ₃ · H ₂ O	H ₂ O	NH ₄ ⁺ · NH ₃ · (H ₂ O) ₂	-53.1	-105
R10	NH ₄ ⁺ · NH ₃ · H ₂ O	NH ₃	NH ₄ ⁺ · (NH ₃) ₂ · H ₂ O	-71.5	-133
R11	NH ₄ ⁺ · (NH ₃) ₂	H ₂ O	NH ₄ ⁺ · (NH ₃) ₂ · H ₂ O	-51.9	-103
R12	NH ₄ ⁺ · (NH ₃) ₂	NH ₃	NH ₄ ⁺ · (NH ₃) ₃	-50	-105
R13	H ₃ O ⁺	H ₂ O	H ₃ O ⁺ · H ₂ O	-136.9	-120
R14	H ₃ O ⁺	NH ₃	NH ₄ ⁺	0	0
R15	H ₃ O ⁺ · H ₂ O	H ₂ O	H ₃ O ⁺ · (H ₂ O) ₂	-84.5	-94
R16	H ₃ O ⁺ · H ₂ O	NH ₃	NH ₄ ⁺	0	0
R17	H ₃ O ⁺ · (H ₂ O) ₂	H ₂ O	H ₃ O ⁺ · (H ₂ O) ₃	-73	-118
R18	H ₃ O ⁺ · (H ₂ O) ₂	NH ₃	NH ₄ ⁺	0	0

¹ $\Delta_r H^0$ and $\Delta_r S^0$ represent the enthalpy and entropy of reaction at standard conditions, respectively. The values are obtained from NIST Chemistry WebBook. Average value is used if more than one measurements are reported. A value of 0 for $\Delta_r H^0$ and $\Delta_r S^0$ means the corresponding reaction is treated as irreversible.

and α -pinene + NH₄ · H₂O are -24 and 11 kJ mol⁻¹, respectively. The reaction entropies of these reactions are assumed to be 0. The simulated dependence of acetone and α -pinene on temperature is shown in Figure S5.

5 Thermodynamic Properties of Selected Analytes

- 90 The proton affinity and NH₄⁺ affinity of selected analytes are shown in Table S2. The NH₄⁺ affinities are really scarce in the literature. Adams et al. (2003) measured the relative NH₄⁺ affinity of four organic compounds. The NH₄⁺ affinity of acetic acid is at least 25 kJ mol⁻¹ smaller than that of acetone, which is 110 kJ mol⁻¹. Thus, the NH₄⁺ affinity of acetic acid is smaller than H₂O (85 kJ mol⁻¹).

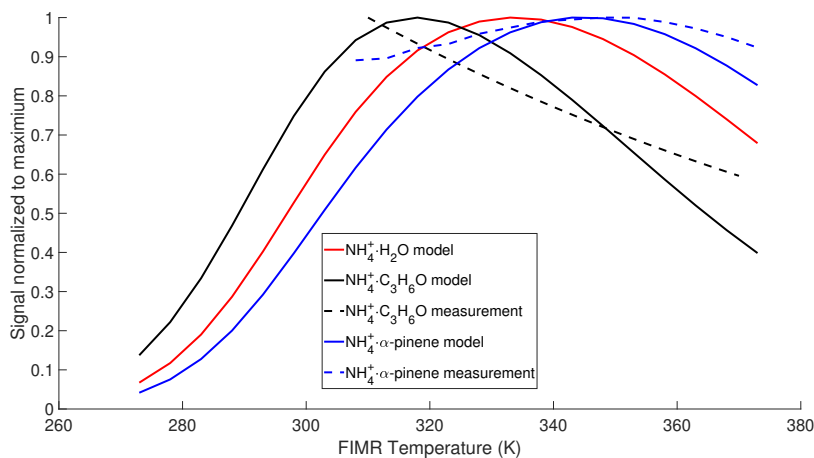


Figure S5. The simulated dependence of acetone and α -pinene signals on FIMR temperature. The signal is normalized to the max.

Table S2. Proton Affinity and NH_4^+ Affinity of selected analytes¹

Analyte	Proton Affinity ²	NH_4^+ Affinity ²
NH_3	853	108
H_2O	691	86
acetone	811	110
α -pinene	863	75
β -pinene	874	76
limonene	842	93
camphene	867	77
benzene	746	80
toluene	782	N/A

¹ The comparison in the NH_4^+ affinity between analyte and H_2O determines whether the ligand-switching reaction between A and $\text{NH}_4^+ \cdot \text{H}_2\text{O}$ is endothermic or exothermic. The comparison in the proton affinity between analyte and NH_3 determines whether the proton transfer reaction between A and $\text{NH}_4^+ \cdot \text{H}_2\text{O}$ is thermodynamically favorable.

² Unit is kJ mol^{-1} . The properties of acetone and monoterpenes are from Canaval et al. (2019). All the other values are from NIST chemistry Web-book.

6 Parameterize the Sensitivity

Figure S6 shows the relationship between observed sensitivity and the ion-molecule collision rate.

The sensitivities of reduced aromatics are really low (< 2 cps ppbv⁻¹) in NH₄⁺ CIMS. This is interesting as the NH₄⁺ affinity of benzene (80 kJ mol⁻¹) is similar to that of α -pinene (75 kJ mol⁻¹), but the sensitivity of α -pinene is 363 cps ppbv⁻¹. We suspect this vast difference in sensitivity is related to the difference in their proton affinity. For both benzene and α -pinene, their NH₄⁺ affinities are lower than that of H₂O, causing their ligand-switching reaction with NH₄⁺ · H₂O endothermic. The energy imparted by the drift voltage could aid the endothermic reaction. Because α -pinene has larger proton affinity than NH₃ (Table S2), NH₄⁺ · α -pinene may undergo an internal proton transfer reaction and transforms to H⁺ · α -pinene · NH₃. This ion may have a larger chance to survive than NH₄⁺ · α -pinene. In contrast, NH₄⁺ · benzene does not undergo this internal proton transfer reaction, because benzene has smaller proton affinity than NH₃. Thus, NH₄⁺ · benzene may quickly break apart in the electric field, leading to the low sensitivity.

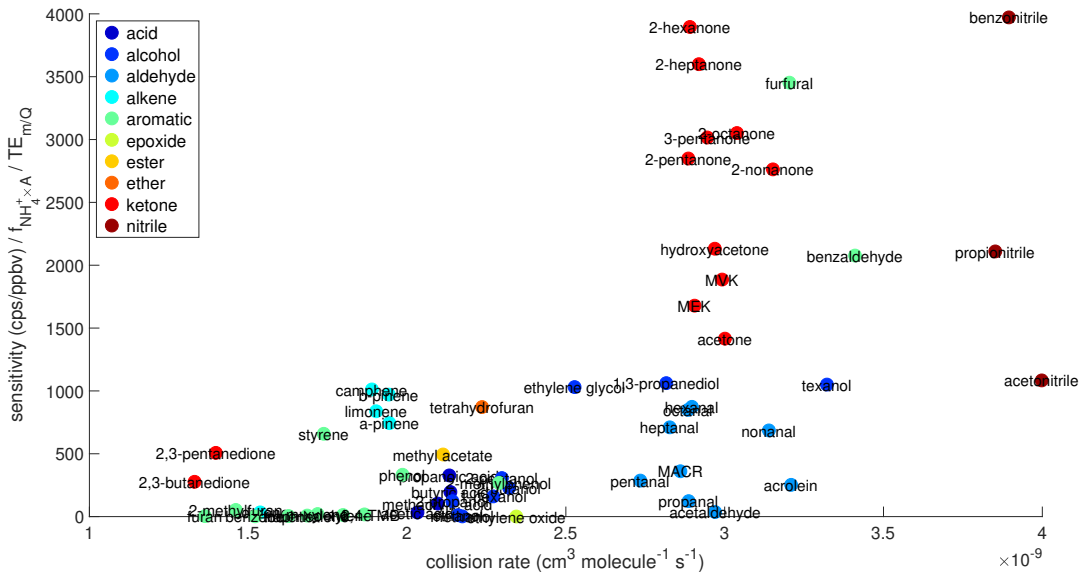


Figure S6. Relationship between sensitivity and ion-molecule collision rate.

7 Instrument Intercomparison

One major disadvantage of CIMS is a lack of isomer separation. If multiple isomers exist for a parent ion and if these isomers are quantified by GC-MS, we apply the GC-MS resolved isomer ratio and the sensitivities of individual isomers to convert the raw cps of the parent ion to the summed mixing ratio of all isomers for NH₄⁺ CIMS, using the derivation below. Assuming parent ion P⁺ is associated with n isomers (isomer_i), with corresponding ambient concentrations ([C_i]) and sensitivities (S_i). The total signal measured by NH₄⁺ CIMS (unit: cps) can be expressed by Eqn. S9, where subscript ref represents an isomer

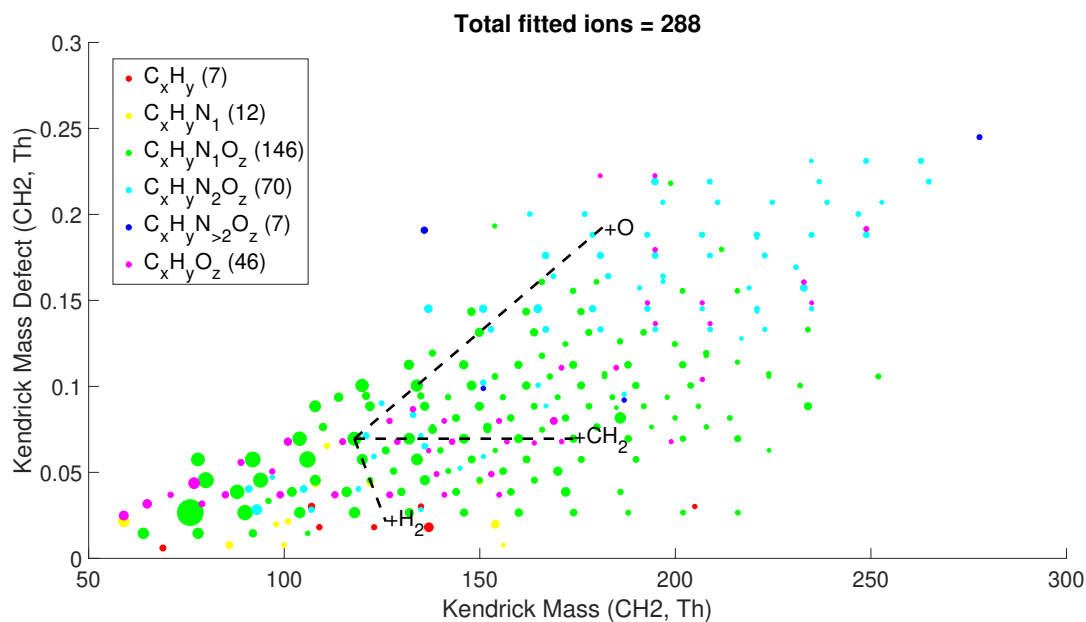


Figure S7. Mass defect plot using CH₂ as reference. The formula shown in the legend contain the reagent ion. Only ions above the detection limit (three standard deviations of measurement background for 1 s integration time) are shown. The symbol size is scaled to the square root of the campaign-averaged signal.

serving as the reference. The concentration ratio of an isomer to the reference isomer (i.e., $\frac{[C_i]}{[C_{ref}]}$) is measured by GC-MS. By rearranging Eqn. S9, we can get $[C_{ref}]$ (Eqn. S10). Finally, the summed concentration of all isomers can be calculated using Eqn. S11.

$$\begin{aligned}
 \text{total signal} &= \sum_1^n ([C_i] \times S_i) \\
 &= [C_{ref}] \sum_1^n \left(\frac{[C_i]}{[C_{ref}]} \times S_i \right)
 \end{aligned} \tag{S9}$$

$$115 \quad [C_{ref}] = \frac{\text{total signal}}{\sum_1^n \left(\frac{[C_i]}{[C_{ref}]} \times S_i \right)} \tag{S10}$$

$$\begin{aligned}
\text{total concentration} &= \sum_1^n ([C_i]) \\
&= [C_{\text{ref}}] \sum_1^n \left(\frac{[C_i]}{[C_{\text{ref}}]} \right) \\
&= \text{total signal} \frac{\sum_1^n \left(\frac{[C_i]}{[C_{\text{ref}}]} \right)}{\sum_1^n \left(\frac{[C_i]}{[C_{\text{ref}}]} \times S_i \right)}
\end{aligned} \tag{S11}$$

Coggon et al. (In prep.) found that several aldehydes, including octanal and nonanal, fragment in the H_3O^+ CIMS and produces $\text{C}_5\text{H}_8\text{H}^+$. The $\text{C}_5\text{H}_8\text{H}^+$ signal from isoprene (i.e., $[\text{C}_5\text{H}_8\text{H}^+]_{\text{isoprene}}$, unit cps) is calculated using Eqn. S12, where $[\text{C}_5\text{H}_8\text{H}^+]$ represents the total signal, $\text{C}_8\text{H}_{14}\text{H}^+$ and $\text{C}_9\text{H}_{16}\text{H}^+$ represent the product ion signals of octanal and nonanal, re-
 120 spectively. The correction factor 7.9 in Eqn. S12 is the ratio of $[\text{C}_5\text{H}_8\text{H}^+]_{\text{total}}$ to $[\text{C}_8\text{H}_{14}\text{H}^+] + [\text{C}_9\text{H}_{16}\text{H}^+]$ at night when the isoprene concentration measured by the GC-MS is low. Correcting such interference results in lower isoprene concentration measured by the H_3O^+ CIMS, particularly at night, and better agreement between H_3O^+ CIMS and GC-MS (Figure 7a).

$$[\text{C}_5\text{H}_8\text{H}^+]_{\text{isoprene}} = [\text{C}_5\text{H}_8\text{H}^+] - 7.9 \times ([\text{C}_8\text{H}_{14}\text{H}^+] + [\text{C}_9\text{H}_{16}\text{H}^+]) \tag{S12}$$

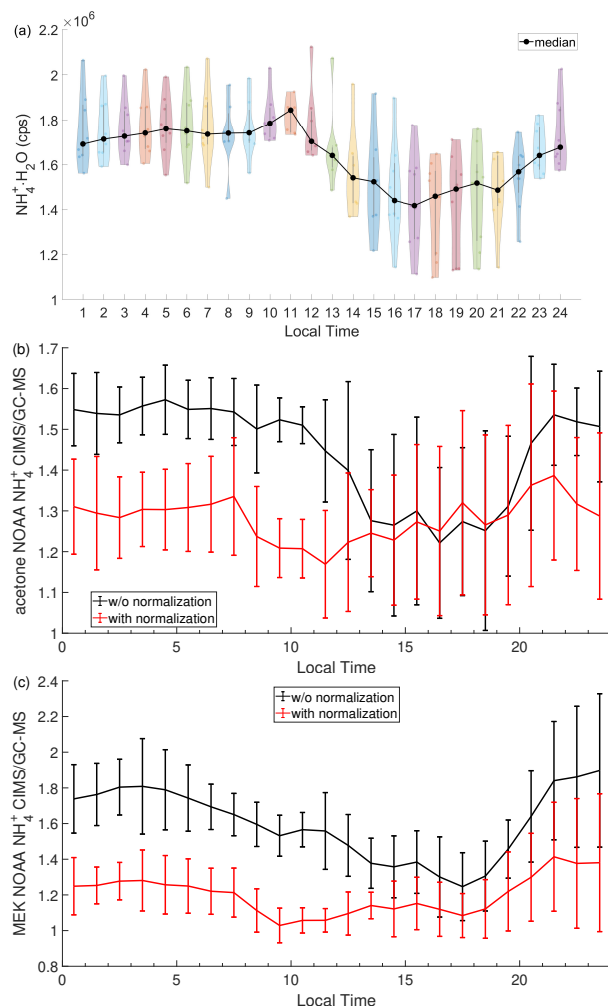


Figure S8. Diurnal trend of (a) reagent ion $\text{NH}_4^+ \cdot \text{H}_2\text{O}$; (b) the ratio of NH_4^+ CIMS to GC-MS for acetone; (c) the ratio of NH_4^+ CIMS to GC-MS for methyl ethyl ketone. Panel (a) is a violin plot.

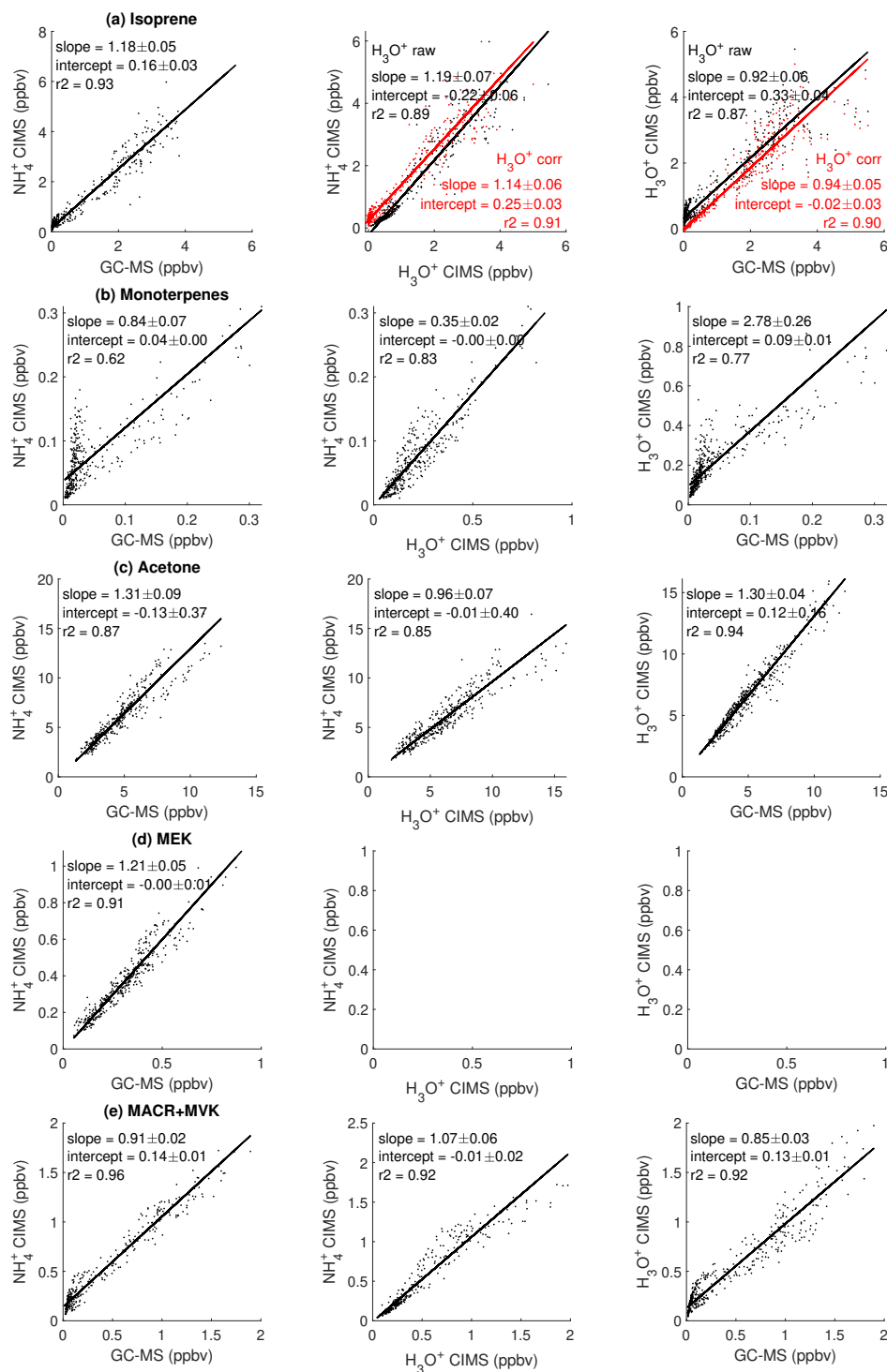


Figure S9. The scatter plot comparison of the concentration of selected species measured by NH_4^+ CIMS, H_3O^+ CIMS, and GC-MS. (a) Isoprene; (b) Monoterpenes; (c) Acetone; (d) Methyl Ethyl Ketone (MEK); (e) Methacrolein (MACR) + Methyl Vinyl Ketone (MVK). MEK measured by the NOAA H_3O^+ CIMS is not included because its peak fitting ($\text{C}_4\text{H}_9\text{O}^+$) is degraded by the nearby large signal of H_3O_4^+ .

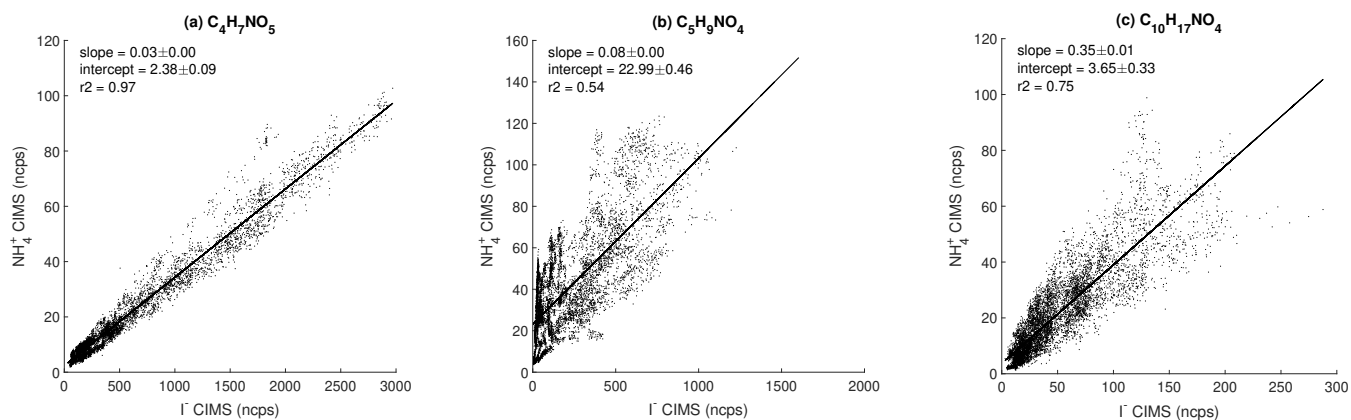


Figure S10. The scatter plot comparison of three nitrogen-containing species measured by NH_4^+ CIMS and I^- CIMS. (a) $\text{C}_4\text{H}_7\text{NO}_5$; (b) $\text{C}_5\text{H}_9\text{NO}_4$; (c) $\text{C}_{10}\text{H}_{17}\text{NO}_4$. Because of a lack of calibration standards, the raw signals (ncps) are shown here.

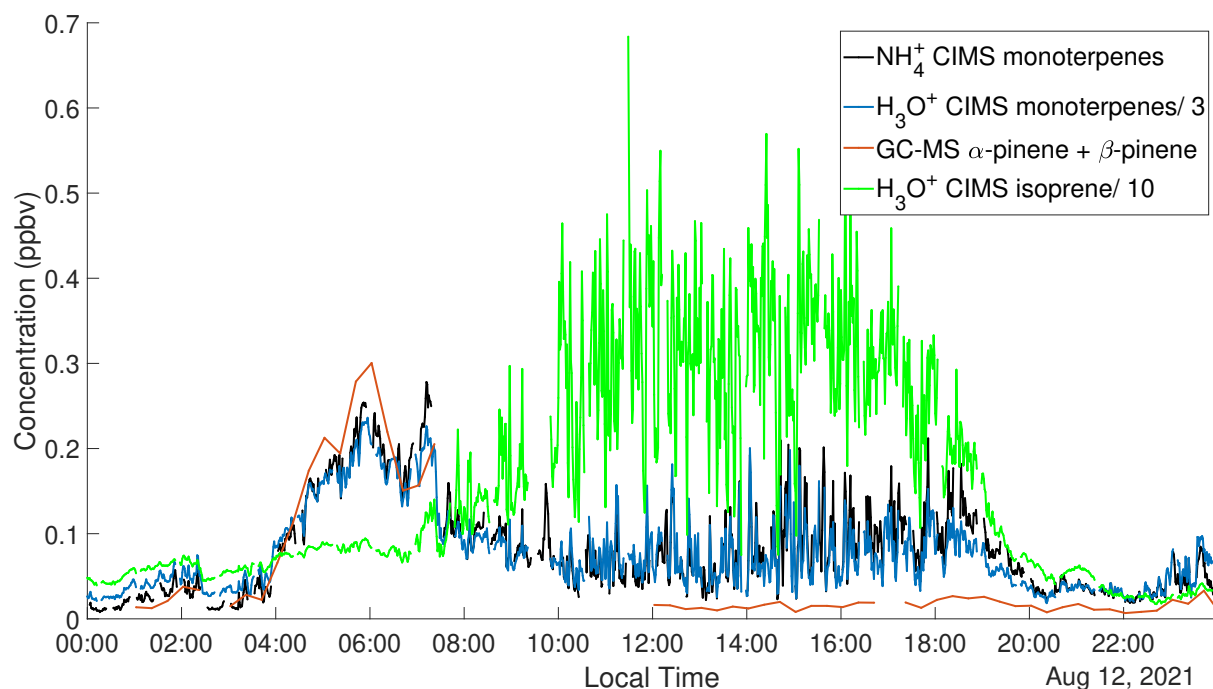


Figure S11. Time series of monoterpenes measured by the NH_4^+ CIMS and H_3O^+ CIMS and isoprene measured by H_3O^+ CIMS for one day. Data shown here have 1 min resolution.

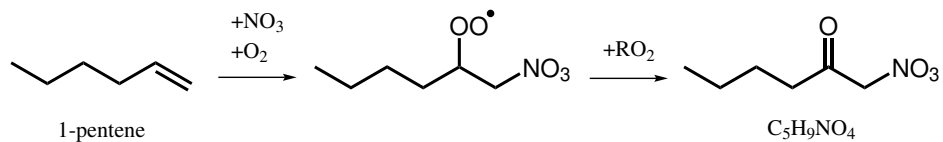


Figure S12. Example formation mechanism of $C_5H_9NO_4$ from the oxidation of 1-pentene by nitrate radical followed by $RO_2 + RO_2$ reaction. Several isomers of nitrooxy carbonyls can be formed from different pentene isomers and different nitrate radical addition positions.

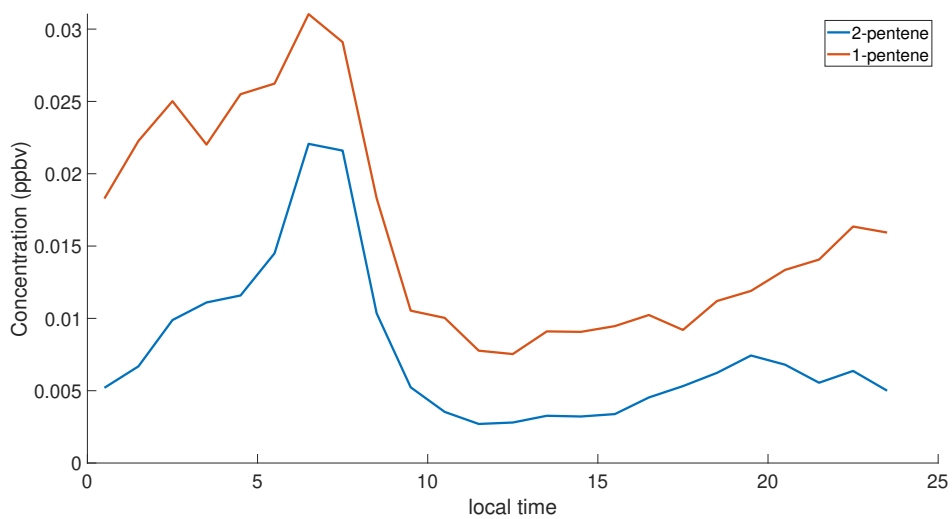


Figure S13. Diurnal trends of pentenes measured by GC-MS.

8 Theoretical Calculations

125 The dipole moment and polarizability of analytes are used to estimate the ion-molecule collision rate constant. These properties of the majority of analytes studied here are from Pagonis et al. (2019). For analytes the properties of which do not exist in that library, we calculate their conformer-weighted dipole moment and the lowest-energy conformer polarizability at the B3LYP/cc-pVTZ level of theory (Garden et al., 2009; Becke, 1993). These analytes are shown in Table S3.

Table S3. Calculated conformer-weighted dipole moment and lowest-conformer polarizability of selected analytes at the B3LYP/cc-pVTZ level of theory (Garden et al., 2009)

Analyte	Polarizability ($\times 10^{-24}\text{cm}^3$)	Dipole moment (D)
furan	6.44	0.61
MVK	7.62	2.92
1,3-propanediol	6.84	2.8
2-methylfuran	8.46	0.59
2,3-butanedione	8.2	0
2-hexanone	11.2	2.73
2,3-pentanedione	9.36	0.19
hexanal	11.8	2.69
benzaldehyde	14.1	3.38
limonene	17.2	0.7
texanol	22.8	3.02

References

- 130 Adams, N. G., Babcock, L. M., Mostefaoui, T. M., and Kerns, M. S.: Selected ion flow tube study of NH_4^+ association and of product switching reactions with a series of organic molecules, *International Journal of Mass Spectrometry*, 223-224, 459–471, [https://doi.org/https://doi.org/10.1016/S1387-3806\(02\)00932-6](https://doi.org/https://doi.org/10.1016/S1387-3806(02)00932-6), 2003.
- Becke, A. D.: Density-Functional Thermochemistry. III. The Role of Exact Exchange, *J. Chem. Phys.*, 98, 5648–5652, <https://doi.org/10.1063/1.464913>, 1993.
- 135 Canaval, E., Hyttinen, N., Schmidbauer, B., Fischer, L., and Hansel, A.: NH_4^+ Association and Proton Transfer Reactions With a Series of Organic Molecules, 7, <https://doi.org/10.3389/fchem.2019.00191>, 2019.
- Coggon, M. C., Stockwell, C. E., Xu, L., and Warneke, C.: PTR interference, In prep.
- Garden, A. L., Paulot, F., Crounse, J. D., Maxwell-Cameron, I. J., Wennberg, P. O., and Kjaergaard, H. G.: Calculation of conformationally weighted dipole moments useful in ion–molecule collision rate estimates, *Chemical Physics Letters*, 474, 45–50, <https://doi.org/https://doi.org/10.1016/j.cplett.2009.04.038>, 2009.
- 140 Heinritzi, M., Simon, M., Steiner, G., Wagner, A. C., Kürten, A., Hansel, A., and Curtius, J.: Characterization of the mass-dependent transmission efficiency of a CIMS, *Atmos. Meas. Tech.*, 9, 1449–1460, <https://doi.org/10.5194/amt-9-1449-2016>, 2016.
- Huey, L. G., Hanson, D. R., and Howard, C. J.: Reactions of SF_6^- and I^- with Atmospheric Trace Gases, *The Journal of Physical Chemistry*, 99, 5001–5008, <https://doi.org/10.1021/j100014a021>, 1995.
- 145 Hunter, E. P. L. and Lias, S. G.: Evaluated Gas Phase Basicities and Proton Affinities of Molecules: An Update, 27, 413–656, <https://doi.org/10.1063/1.556018>, 1998.
- Kawai, Y., Yamaguchi, S., Okada, Y., Takeuchi, K., Yamauchi, Y., Ozawa, S., and Nakai, H.: Reactions of protonated water clusters $\text{H}+(\text{H}_2\text{O})_n$ ($n=1-6$) with dimethylsulfoxide in a guided ion beam apparatus, *Chemical Physics Letters*, 377, 69–73, [https://doi.org/https://doi.org/10.1016/S0009-2614\(03\)01095-9](https://doi.org/https://doi.org/10.1016/S0009-2614(03)01095-9), 2003.
- 150 Lopez-Hilfiker, F. D., Iyer, S., Mohr, C., Lee, B. H., D'Ambro, E. L., Kurtén, T., and Thornton, J. A.: Constraining the sensitivity of iodide adduct chemical ionization mass spectrometry to multifunctional organic molecules using the collision limit and thermodynamic stability of iodide ion adducts, *Atmos. Meas. Tech.*, 9, 1505–1512, <https://doi.org/10.5194/amt-9-1505-2016>, 2016.
- Pagonis, D., Sekimoto, K., and de Gouw, J.: A Library of Proton-Transfer Reactions of H_3O^+ Ions Used for Trace Gas Detection, *Journal of the American Society for Mass Spectrometry*, 30, 1330–1335, <https://doi.org/10.1007/s13361-019-02209-3>, 2019.
- 155 Zaytsev, A., Breitenlechner, M., Koss, A. R., Lim, C. Y., Rowe, J. C., Kroll, J. H., and Keutsch, F. N.: Using collision-induced dissociation to constrain sensitivity of ammonia chemical ionization mass spectrometry (NH_4^+ CIMS) to oxygenated volatile organic compounds, *Atmos. Meas. Tech.*, 12, 1861–1870, <https://doi.org/10.5194/amt-12-1861-2019>, 2019.